atmosphere

MDPI

Article

Sensitivity of Vegetation Productivity to Extreme Droughts across the Yunnan Plateau, China

Chen Lin, Yunling He * and Zhenyan Wang

School of Earth Sciences, Yunnan University, Kunming 650091, China; lc18959472907@mail.ynu.edu.cn (C.L.); wangzhenyan1@stu.ynu.edu.cn (Z.W.)
* Correspondence: yunling@ynu.edu.cn; Tel.: +86-13708881061

Abstract: Extreme drought has negative impacts on the health of vegetation and the stability of ecosystems. In this study, the CASA model was employed to estimate the net primary productivity of vegetation over the Yunnan Plateau. The time-lag effects on vegetation were observed within a 0–6 month period of extreme droughts using the Pearson correlation coefficient. The resistance of vegetation during extreme droughts was quantified, and the recovery capability of vegetation following these events was analyzed using the ARIMA model. Moreover, the study investigated the response of vegetation to extreme droughts across diverse altitudinal gradients. The results showed that: (1) This round of extreme drought led to a decrease in the NPP of vegetation in the Yunnan Plateau. (2) Vegetation exhibits a 1–3-month lag period in response to extreme drought, with forests showing slower responses than grasslands and shrubs and higher resistance to the drought. Except for agricultural vegetation, most other vegetation types are able to recover their productivity within a year. (3) Vegetation above 3000 m is less susceptible to the impacts of extreme drought. With increasing elevation, forests exhibit an earlier lag period in response to extreme drought and an increase in resistance, but lower elevation vegetation demonstrates better recovery from extreme drought events. Shrub vegetation shows the highest resistance at elevations between 3000–4000 m, and shrubs at middle to high elevations have better recovery capacity than those at low elevations. Grassland vegetation exhibits increased resistance to extreme drought with higher elevation and shows better recovery. Agricultural vegetation demonstrates higher resistance at middle to high elevations, with no significant elevation differences in recovery capacity. Extreme drought events not only have a lag effect on the vegetation ecosystem, but also affect its stability and resilience to future drought events. To adapt to climate change, future research should emphasize the role of small-scale climate in vegetation's response to drought.

Keywords: net primary productivity (NPP); extreme drought; elevation gradient; time-lag effect; resilience; resistance

Citation: Lin, C.; He, Y.; Wang, Z. Sensitivity of Vegetation Productivity to Extreme Droughts across the Yunnan Plateau, China. *Atmosphere* **2023**, *14*, 1026. https://doi.org/10.3390/atmos14061026

Academic Editors: Huaiyong Shao, Jinping Liu and Huaan Jin

Received: 29 May 2023
Revised: 9 June 2023
Accepted: 12 June 2023
Published: 15 June 2023

1. Introduction

Global climate change has intensified in recent years, causing more frequent extreme droughts [1]. These droughts limit plant growth, weaken carbon storage, and destabilize ecosystems [2–4]. They pose significant risks to plant communities and socioeconomic aspects [5,6]. Net primary productivity (NPP) reflects the natural production capacity of vegetation, indicating ecosystem quality [7]. It is a crucial indicator for assessing ecosystem health. Understanding NPP's spatial and temporal distribution and its response to extreme droughts is vital for protecting the environment and achieving sustainable development amidst rapid global climate change.

Currently, research on the effects of extreme drought on vegetation primarily focuses on ecosystem functionality, vegetation growth, and physiological responses. Studies have shown that drought can lead to land degradation, exacerbate the loss of plant habitats, and result in biodiversity loss [8–10]. These impacts have significant consequences for

human society, the economy, and ecosystems. In terms of identifying extreme drought disasters, a commonly used method is to establish various meteorological drought indices based on threshold identification using meteorological data, such as SPI, SPEI, SCDHI, etc. [11,12]. Regarding vegetation responses to extreme drought, current research suggests that the global vegetation response to climate change is complex. The mechanisms by which extreme drought affects vegetation productivity are still subject to considerable debate. Some studies suggest that large-scale drought is a major driver of global decline in NPP [13]. However, changes in vegetation greenness are not affected by short-term water shortages, and the response of vegetation to drought is slow [14]. Moreover, vegetation gradually exhibits adaptability to climate warming [15], and there are regional differences in the response to climate change [16], with varying and sometimes opposing trends observed under different water and thermal conditions. For instance, in humid environments, elevated temperatures can promote net carbon absorption by ecosystems, while in arid environments, it can inhibit net carbon absorption [17]. In wet regions such as the Amazon rainforest, photosynthesis and productivity of vegetation often increase with increasing drought severity [18,19]. Furthermore, it has been found that drought primarily affects the NPP of sparse vegetation, making dry and semi-arid regions more vulnerable to its impacts [20,21]. Meanwhile, elevation is considered an important factor influencing the sensitivity of vegetation productivity to extreme drought conditions. The lingering effects of extreme drought on vegetation greenness exhibit a clear dependence on elevation. The impact of drought on vegetation greenness decreases with decreasing elevation [22,23]. Extreme dry weather has little effect on vegetation productivity in high-elevation areas but exerts a strong negative influence on warm-season vegetation productivity in low-elevation regions [24].

The response of vegetation to climate change varies regionally due to factors such as geographical location, topography, soil type, and vegetation type. The Yunnan Plateau, with its complex topography and significant elevation differences, exhibits rich climatic diversity. Current research on vegetation in the Yunnan Plateau is mostly based on NDVI and LAI [25–27], which primarily focus on the growth status and coverage of vegetation. However, studies on NPP, which reflects plant productivity and ecological functionality, are still lacking. Existing studies only indicate that drought can lead to a decline in NPP in the Yunnan Plateau and that different vegetation types exhibit varying sensitivities [28,29]. There is still a lack of comprehensive research on the impact of extreme droughts on vegetation productivity, particularly considering the role of altitudinal gradients. Therefore, in this study, we utilized the CASA model to estimate the NPP of vegetation in the Yunnan Plateau. We investigated the vegetation productivity response to extreme droughts in three stages: lagged effects, resistance, and recovery capability. Lagged effects were analyzed using the Pearson correlation coefficient to examine the delayed response of vegetation to extreme droughts within a 0–6 month period. Vegetation resistance during extreme droughts was calculated, and the recovery capability of vegetation after the occurrence of extreme droughts was analyzed using the ARIMA model. Furthermore, we explored the influence of altitude on these effects. This study delves into the response patterns of vegetation in the Yunnan Plateau to drought. It offers new research perspectives to assess vegetation response patterns and aims to enhance our overall comprehension of the impact of global climate change on vegetation ecosystems.

2. Materials and Methods

2.1. Study Area

The Yunnan Plateau is located in southwest China, neighboring Guizhou and Guangxi Provinces on the east and connected to Sichuan Province on the north (Figure 1a). Its total area is 394,100 square kilometers, and the permanent population is 46.9 million. Most of the areas are between 1000 and 3500 m above sea level. It belongs to the mountainous plateau terrain, which is high in the northwest and low in the southeast and has rich vegetation types (Figure 1b). Its climate basically belongs to the subtropical plateau monsoon type. The

hottest month in the Yunnan Plateau is July, with an average temperature of 19~22 °C. The coldest month is January, with an average temperature of 6~8 °C or less. The temperature changes vertically with the height of the terrain. The distribution of precipitation in the province is uneven in terms of seasons and regions. At the same time, the Yunnan Plateau spans across 10 latitude zones and 7 climatic zones, with an elevation difference of over 6000 m. The complex topography and significant elevation differences create different climatic zones in the Yunnan Plateau, resulting in rich climatic diversity. This topography also influences the direction and speed of airflows, further affecting the distribution of precipitation [30]. Influenced by the Southwest Monsoon and the Tibetan Plateau's impact on the atmospheric circulation system, the precipitation distribution in the Yunnan Plateau is uneven, with distinct dry and wet seasons and significant seasonal variations in drought [31]. Despite relatively moderate temperatures, the Yunnan Plateau experiences strong solar radiation and low wind speeds, and is situated in a karst landform area with high permeability and low soil water-holding capacity, making it highly vulnerable to drought events [32,33].

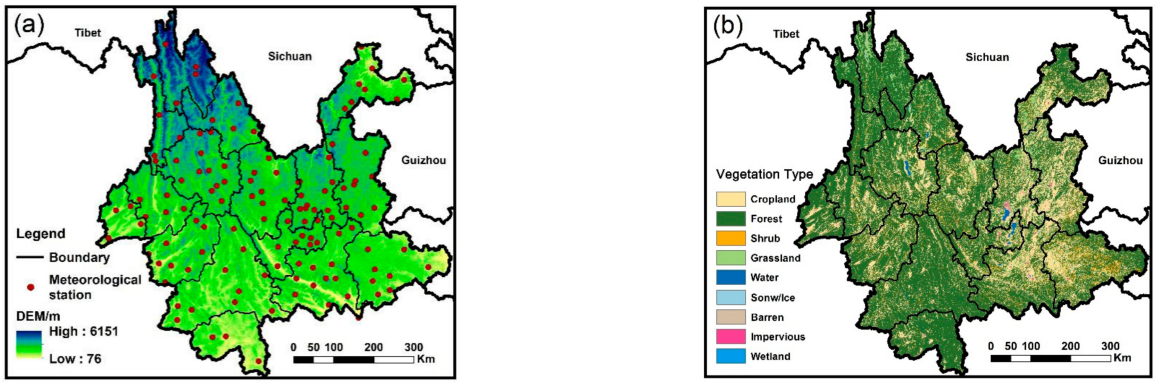

(**a**) (**b**)

Figure 1. Topographic map and vegetation types on Yunnan Plateau. (**a**) Topographic map. (**b**) Vegetation types.

2.2. Data

The meteorological data included monthly records of the minimum temperature (T_{min}), maximum temperature (T_{max}), average temperature (T_{ave}), precipitation (Pre), sunshine duration (SSD), atmospheric pressure (P), and wind speed at a height of 2 m (U_2) at the Yunnan provincial meteorological stations from 1982 to 2019. These data were obtained from the Resource and Environment Science and Data Center of the Chinese Academy of Sciences (https://www.resdc.cn/ (accessed on 1 January 2023)). After excluding stations with migration records and conducting quality checks, we finally selected meteorological data from 125 stations in Yunnan Plateau for calculations. In order to meet the data requirements of the Carnegie–Ames–Stanford approach (CASA) model in the simulation of NPP, we employed Tong's formula [34] to convert sunshine duration into solar radiation. Due to the large altitudinal differences and complex terrain in Yunnan, we introduced elevation as a covariate and utilized the ANUSPLIN software for interpolation to achieve better results. ANUSPLIN is a specialized software for fitting climate data surfaces (developed by Australian scientist Hutchinson) based on thin plate spline theory [35]. It allows for the incorporation of multivariate covariate linear submodels and is particularly suitable for time series meteorological data. It has demonstrated superior interpolation accuracy compared to other methods in regions with complex terrains [36] and has been widely studied and applied [37–39]. After interpolation, we obtained a grid dataset of monthly average temperature, monthly average precipitation, and monthly total solar radiation from 1982 to 2019, with a spatial resolution of 500 m.

The normalized difference vegetation index (NDVI) required for calculating NPP in the CASA model was selected from the MOD13Q1 provided by the US National Aeronautics and Space Administration (NASA) data center. This dataset provides NDVI products with a spatial resolution of 250 m and a temporal resolution of 16 days from 2001 to 2019. We resampled and clipped the original products and used the maximum value composite (MVC) method to composite the biweekly NDVI data into monthly sequences. The NDVI data from 1982 to 2000 was selected from AVHRR NDVI. In addition to the previously mentioned processing steps, to ensure that the input resolution of the CASA model remains consistent, we used the code from Ma et al.'s paper to resample the NDVI to 500 m spatial resolution [40].

The land use types required for calculating NPP in the CASA model were selected from the Chinese land cover dataset (CLCD) based on Landsat from 1985 to 2019 [41]. The data were classified using a random forest classifier and further improved in accuracy through temporal and spatial filtering and logical inference operations. The dataset has a spatial resolution of 30 m and a temporal resolution of one year. We resampled and clipped the data to obtain annual land cover type data for the Yunnan Plateau at a spatial resolution of 500 m, which is suitable for our analysis.

2.3. Methods

2.3.1. Identification of Extreme Drought Disasters

The three-month scale SPEI (SPEI-3) is calculated by standardizing the precipitation and evapotranspiration data over the past three months. It is based on the Thornthwaite equation and the calculation method of the standardized precipitation index (SPI), aiming to reflect the balance between precipitation and evapotranspiration. Considering the influence of the Southwest Monsoon and the Tibetan Plateau on the atmospheric circulation system, the distribution of precipitation in the Yunnan Plateau is uneven, with distinct dry and wet seasons. Drought exhibits significant seasonal variations. Therefore, we chose SPEI-3 to identify drought events. The calculation steps can be referred to in the literature [42]. Among them, potential evapotranspiration (ET_0) was calculated using the Penman–Monteith model revised by the Food and Agriculture Organization (FAO) according to the following formula:

$$ET_0 = \frac{0.408\Delta(R_n - G) + \gamma\frac{900}{T+273}U_2(e_s - e_a)}{\Delta + \gamma(1 + 0.34U_2)} \quad (1)$$

where ET_0 is the potential evapotranspiration, mm/d; R_n is net radiation, MJ/(m·d); G is the soil heat flux density, MJ/(m^2 d); γ is the dry–wet constant, kPa/°C; Δ is the slope of the saturated water vapor pressure curve, kPa/°C; U_2 is the wind speed at a height of 2 m, m/s; e_s is the average saturated water vapor pressure, kPa; e_a is the actual water vapor pressure, kPa; and T is the average temperature, °C.

To evaluate the overall drought situation in Yunnan, we computed the mean value of SPEI-3 ($SPEI_{ave\text{-}3}$) using data from 125 meteorological stations in the province. $SPEI_{ave\text{-}3} < 0$ indicated the occurrence of drought events in Yunnan for the corresponding month. The spatial distribution of Yunnan's SPEI-3 was obtained by interpolating the data from 125 meteorological stations. According to the national standard, "Meteorological Drought Grades (GB/T 20481-2017)" established by the China National Climate Center, we define SPEI < −1.5 as regions experiencing extreme drought events. We calculated the proportion of the area of pixels with extreme drought events in relation to the total area of pixels as the proportion of the area affected by extreme drought in the Yunnan Plateau. The frequency of extreme drought events was calculated by counting the number of months when SPEI-3 < −1.5. In addition, the relative intensity of drought (I) was obtained by

performing a min-max standardization and normalization process on SPEI-3 with the following calculation formula:

$$I' = 1/\left(\frac{SPEI - SPEI_{min}}{SPEI_{max} - SPEI_{min}}\right) \quad (2)$$

$$I = \frac{I - I_{min}}{I_{max} - I_{min}} \quad (3)$$

where I' is the SPEI index after standardization; $SPEI_{max}$ is the maximum pixel value of the SPEI grid; $SPEI_{min}$ is the minimum pixel value of the SPEI grid; and I is the relative intensity of drought (the range of I is from 0 to 1, with values closer to 1 indicating greater drought intensity).

2.3.2. CASA Model for Estimating NPP in Yunnan Plateau

Net primary productivity (NPP) of vegetation refers to the amount of organic matter accumulated by green plants per unit area and per unit of time. It can reflect the productivity of vegetation communities under natural environmental conditions and characterize the quality status of terrestrial ecosystems. We used the CASA model to calculate NPP. The specific calculation procedure can be consulted in this paper: [16]. The estimation formula is as follows:

$$NPP(x,t) = APAR(x,t) \times \varepsilon(x,t) \quad (4)$$

In the formula, *APAR(x, t)* represents the photosynthetically active radiation absorbed by pixel x in t month ($gC \cdot m^{-2} \cdot month^{-1}$), and *ε(x, t)* represents the actual light energy utilization rate of pixel x in t month ($gC \cdot MJ^{-1}$).

2.3.3. The Lagged Response of Vegetation to Extreme Drought

Plants exhibit a lagged response in NPP when encountering extreme drought events, rather than an immediate one. Pearson correlation measures linear correlation between two variables. We used it to calculate the correlation between the NPP and SPEI index with a 0–6 month lag.

$$R_{xy} = \frac{\sum_{i=1}^{n}(x_i - \overline{x})(y_i - \overline{y})}{\sqrt{\sum_{i=1}^{n}(x_i - \overline{x})^2 \sum_{i=1}^{n}(y_i - \overline{y})^2}} \quad (5)$$

$$R_i = corr(\mathrm{SPEI_n}, \mathrm{NPP_{n-i}}); 0 \leq i \leq 6 \quad (6)$$

Here, R_i is the Pearson correlation coefficient with a lag of i months during extreme drought periods; NPP is the monthly NDVI time series during extreme drought periods; and SPEI is the corresponding SPEI-3 time series. The lag time, i, corresponding to the maximum Pearson correlation coefficient is the time lag of NPP in response to drought.

2.3.4. The Resistance of Vegetation to Extreme Drought

Vegetation's ability to maintain its original NPP during extreme drought is called resistance, which can be calculated using the following formula:

$$R_{resist} = \frac{NPP_i - \overline{NPP}_{Non-drought}}{\overline{NPP}_{Non-drought}} \quad (7)$$

where, R_{resist} is resistance of NPP to extreme drought; NPP_i is the NPP value during extreme drought; and $\overline{NPP}_{Non-drought}$ is the average NPP value during non-drought periods. A higher R_{resist} indicates stronger resistance.

2.3.5. The Recovery Ability of Vegetation after Extreme Drought

Vegetation resilience refers to recovering normal productivity levels after extreme drought. An extreme drought changes NPP and creates a relative error (E_{error}) between the

true NPP (NPP_{true}) and theoretical NPP (NPP_{pred}) without drought, which represents the drought's impact on NPP. When the impact of extreme drought decreases and the relative error falls within the "acceptable range" for the first time, it represents the vegetation recovering to its normal level. We used the autoregressive integrated moving average (ARIMA) model to predict the theoretical NPP (NPP_{pred}) without extreme drought. The "acceptable range" referred to the range of theoretical NPP after error correction. The ARIMA model is a time series analysis method proposed by Box and Jenkins that combines autoregressive (AR) and moving average (MA) models that consider differencing (integrated) and can predict different types of time series [43].

The formula for calculating vegetation's resilience to extreme drought is as follows:

$$E_{error} = \frac{NPP_{true} - NPP_{pred}}{\overline{NPP}_{true}} \tag{8}$$

When the error between the actual value and the theoretical normal value of NPP falls within the "acceptable range," it indicates that the vegetation has started to recover, represented by:

$$\frac{NPP_{pred} + \sigma - NPP_{true}}{\overline{NPP}_{true}} < 0 \tag{9}$$

Among which:

$$\sigma = \frac{\sum_{i=1}^{n}\left(NPP_{true} - NPP_{pred}\right)}{\overline{NPP}_{true}} \tag{10}$$

where E_{error} is the relative error between the true value and the theoretical normal value, NPP_{true} is the true value calculated by the CASA model, NPP_{pred} is the theoretical value calculated by the ARIMA model, and $\overline{NPP}_{true}$ is the average of true values during the prediction period. σ is the correction coefficient.

The formula simplified is as follows:

$$E_{Corr\_error} = E_{error} - \sigma > 0 \tag{11}$$

We define the time when the corrected relative error (E_{Corr_error}) first exceeds 0 as the time when vegetation has recovered to normal productivity.

The flowchart of this study is shown in Figure 2.

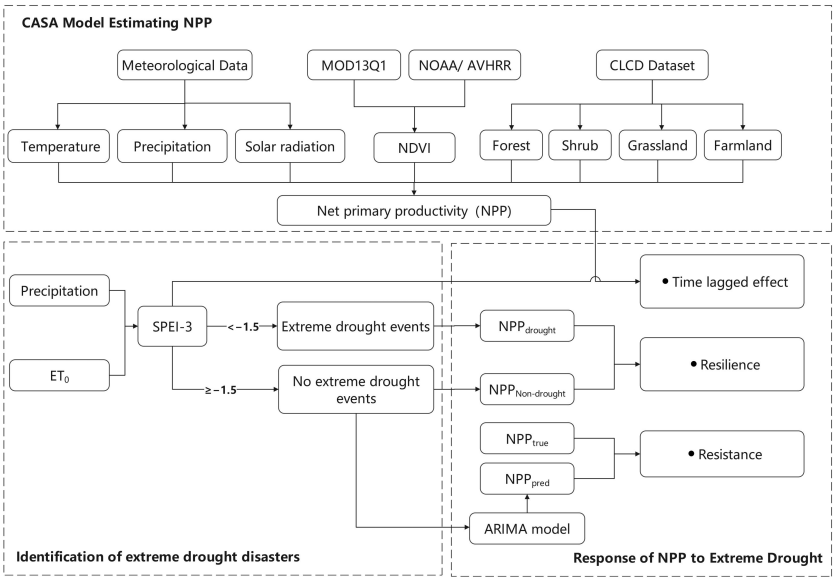

Figure 2. Research flowchart.

3. Results

3.1. Spatial-Temporal Distribution of Drought Disasters and NPP in Yunnan Plateau

Figure 3a shows the $SPEI_{ave\text{-}3}$ in the Yunnan Plateau from 1982 to 2019, indicating that the Yunnan Plateau is susceptible to drought, with periodic drought events occurring every few years. The area affected by extreme droughts typically ranges from 0–40%, but in some severe drought months, such as the beginning of 1984, around 2010, and mid-2019, it can exceed 60% (Figure 3b). Drought intensity is higher in the central and northwest regions than in the southern part of the Yunnan Plateau, with a higher frequency of extreme drought events (Figure 3c,d). According to the historical disaster records in publications such as the *Yunnan Disaster Reduction Yearbook (1991–2018)*, *China Meteorological Disaster Yearbook (2004–2019)*, and *Analysis of Major Drought Events in China (1961–2020)*, strong drought events occurred in the Yunnan Plateau in years such as 1987, 1992, 2008, and 2019. These historical disaster records are consistent with the results of this study. By analyzing the drought intensity and affected area comprehensively, the period from September 2009 to April 2010 had the strongest drought intensity, largest affected area, and longest duration (Figure 3e), and was selected for this study's analysis of the impact of extreme drought events on NPP.

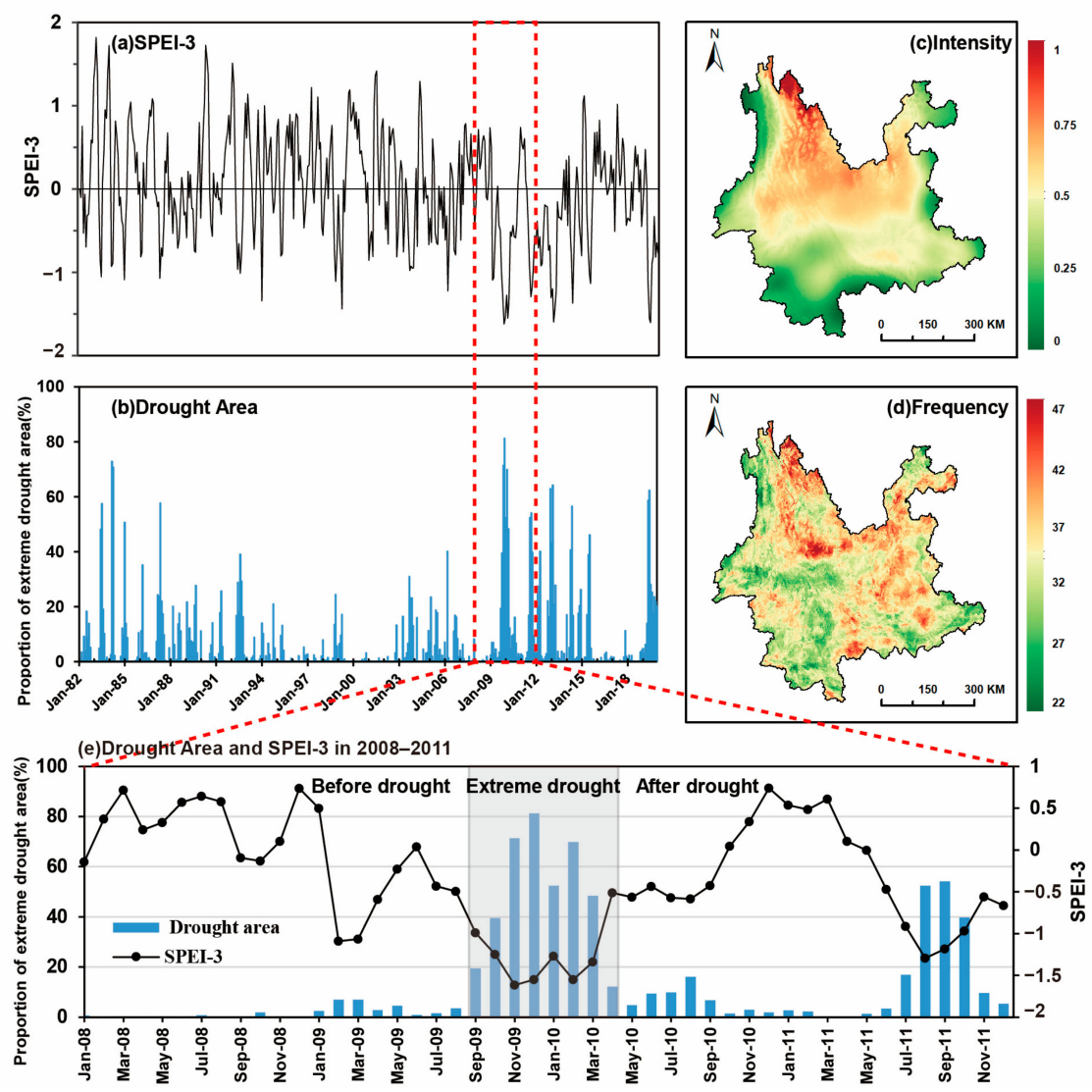

Figure 3. The spatiotemporal distribution of drought intensity, area, and frequency in the Yunnan Plateau.

Figure 4a–f show the spatial and temporal distribution of the SPEI-3 index and monthly mean NPP from September 2008 to August 2009 (one year before the extreme drought), from September 2009 to April 2010 (during the extreme drought), and from May 2010 to May 2011 (one year after the extreme drought). One year before the extreme drought, most areas in the Yunnan Plateau had a SPEI-3 greater than −0.5, indicating almost no drought events occurred in the entire province. From September 2009 to April 2010, an extremely severe drought event occurred in central and eastern Yunnan, with SPEI values lower than 1.5 in most areas. One year after the extreme drought, there were still some localized mild drought events in the central and eastern regions of Yunnan (Figure 4a–c). NPP distribution in the Yunnan Plateau decreased from south to north and from west to east, with the highest NPP values in Xishuangbanna Dai Autonomous Prefecture and Pu'er City reaching over 90 gC·m^{-2}·month^{-1}. The northwestern Hengduan Mountains, water bodies, and canyon areas had lower NPP values with an average below 60 gC·m^{-2}·month^{-1} (Figure 4d–f). NPP decreased during the extreme drought, particularly in central and eastern Yunnan, and then recovered one year after the extreme drought.

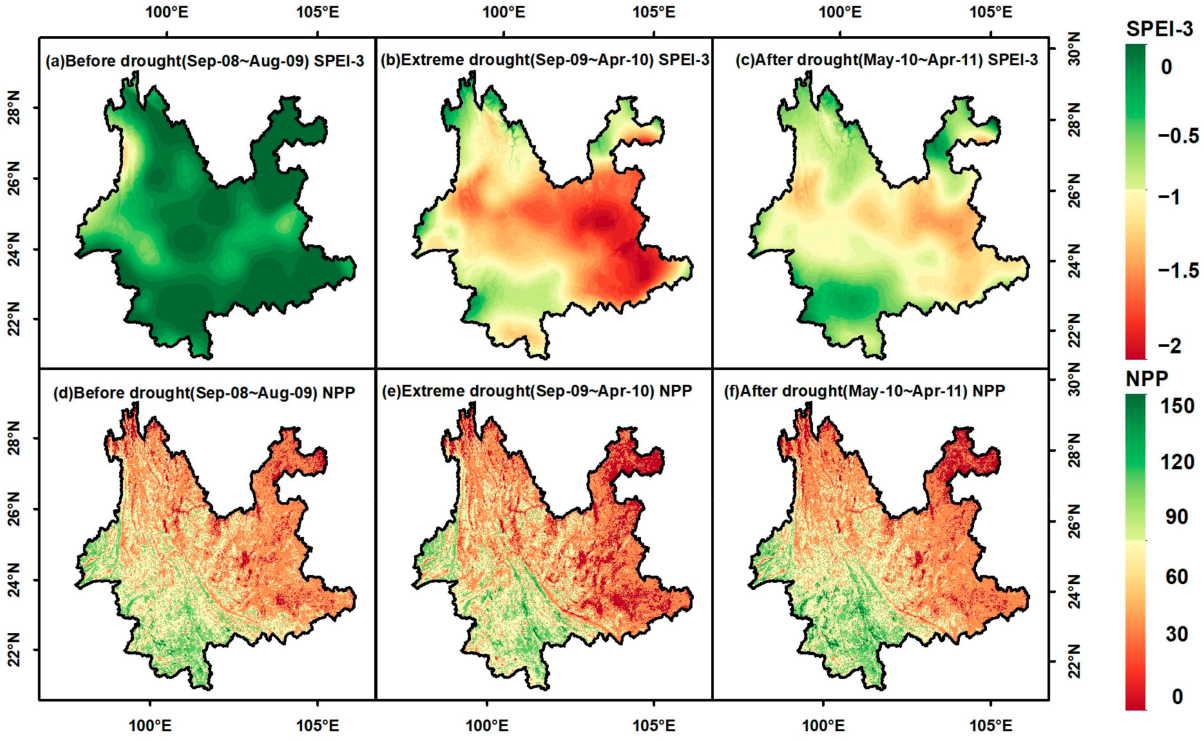

Figure 4. Spatial distribution of SPEI-3 and NPP during the extreme drought, one year before, and one year after the extreme drought.

We further conducted statistical analysis of the changes in NPP of forests, shrubs, grasslands, and farmland at different elevations during the extreme drought and the year before and after the extreme drought (Figure 5). Ranking different vegetation types, forest NPP > farmland NPP > grassland NPP > shrub NPP. The NPP of forests, shrubs, and grasslands increased with the elevation, and NPP was highest at an elevation of 2000–3000 m, followed by a decrease with the decrease in elevation. The NPP of farmland showed the highest value at low elevations and decreased with the increase in elevation. During the extreme drought period, the difference in NPP between low-elevation vegetation and pre-extreme drought NPP was greater than that of high-elevation vegetation, indicating that low-elevation vegetation was more susceptible to drought, resulting in a decrease in NPP. The difference in NPP of low-elevation vegetation before and after the extreme drought was smaller than that of high-elevation vegetation, indicating that the recovery

of NPP of low-elevation vegetation affected by drought was better than that of high-elevation vegetation.

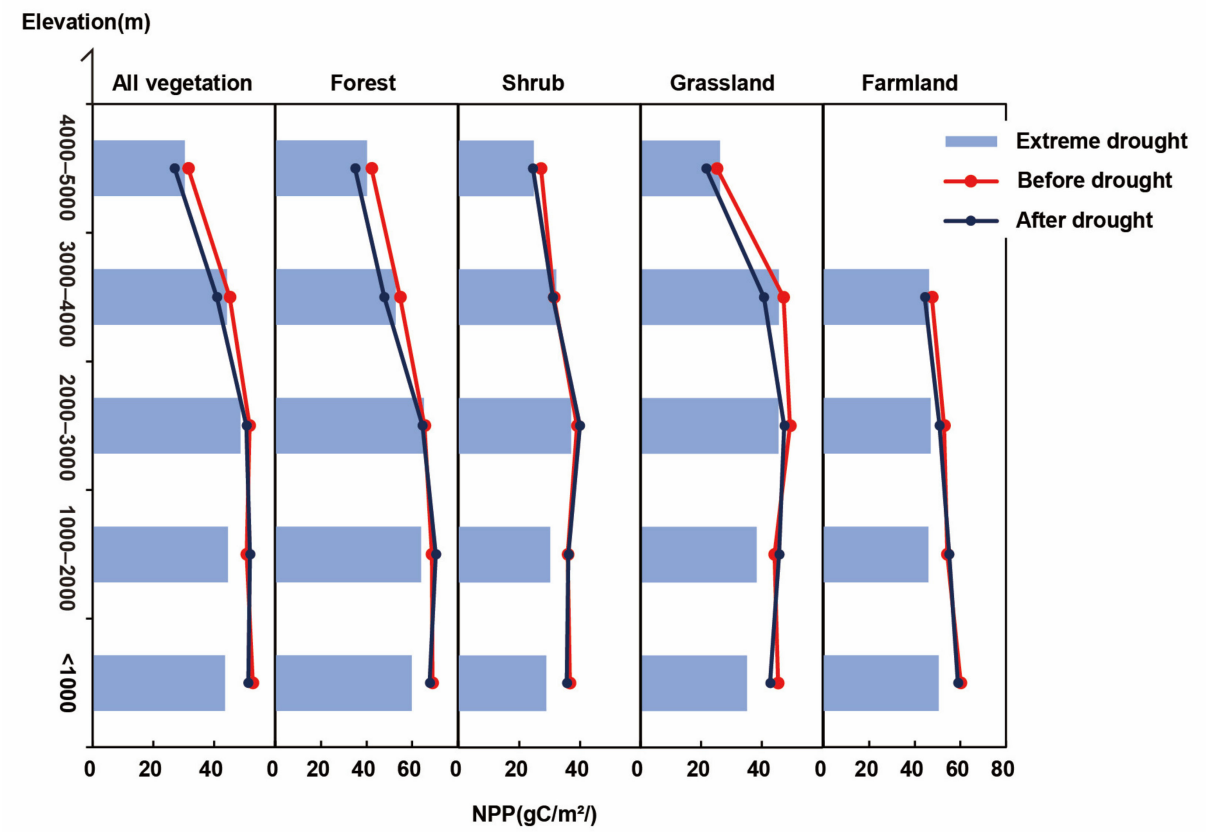

Figure 5. Changes in NPP of different vegetation types before and after drought.

3.2. Lag Effects of Vegetation on Extreme Drought

The lag effect of vegetation response to extreme drought was investigated. Pearson correlation analysis was used to calculate the correlation coefficients between the 0–6 month lagged SPEI-3 and NPP in each grid cell. As shown in Figure 6, a strong positive correlation between SPEI-3 and NPP was observed at a lag time of 1–3 months, with the positive correlation mainly concentrated in the central part of the Yunnan Plateau, indicating a high correlation between NPP changes and drought in this area. However, at a lag time of 6 months, the correlation between SPEI-3 and NPP was mostly negative or not significant. Further analysis of the correlation between SPEI-3 and NPP for different vegetation types at different elevation gradients (Figure 7) indicated that vegetation types below 3000 m exhibited a higher positive correlation at a lag time of 1–3 months, while those above 3000 m showed a lower correlation. For forest vegetation, the lag time of vegetation response to drought was about 2–3 months at elevations below 1000 m, which advanced with increasing elevation, and showed a lower correlation between drought and vegetation response above 3000 m. For shrubs, grasslands, and farmland below 3000 m, the lag time was between 1–3 months, while above 3000 m, a lower correlation was observed.

3.3. Resistance of Vegetation to Extreme Drought

The ability of vegetation to maintain its original level when affected by drought is called resistance. The resistance of different vegetation at different elevation gradients was calculated, and the results are shown in Figure 8. The results indicate that as elevation increases, the resistance of vegetation to drought increases. When subdividing different vegetation types, the order of resistance from high to low is forest > grassland > farmland > shrubland. For forest and grassland vegetation, the resistance to drought increases

with elevation. Although the average resistance value of vegetation at 4000–5000 m is the highest, the range of resistance variability is large, indicating that the resistance of forest and grassland vegetation to drought in high-elevation areas shows greater differences. For shrub vegetation, the resistance increases with elevation below 3000 m, with the highest resistance at 3000–4000 m, and a decrease in resistance at elevations of 4000–5000 m. For farmland vegetation, the resistance to drought is the lowest at 1000–2000 m, and relatively high at 2000–4000 m.

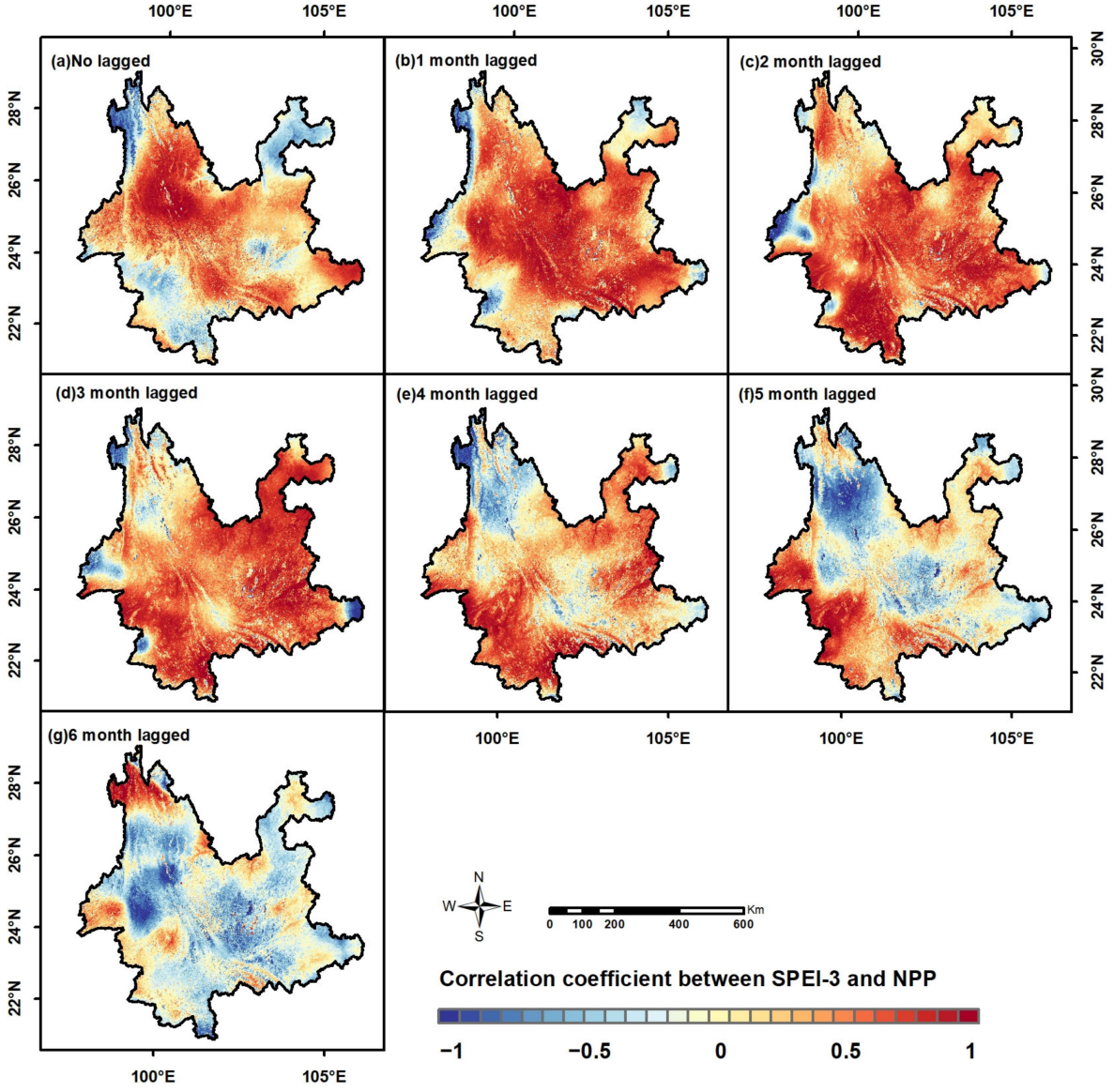

Figure 6. Correlation between SPEI and NPP with different lag months for vegetation at different elevations.

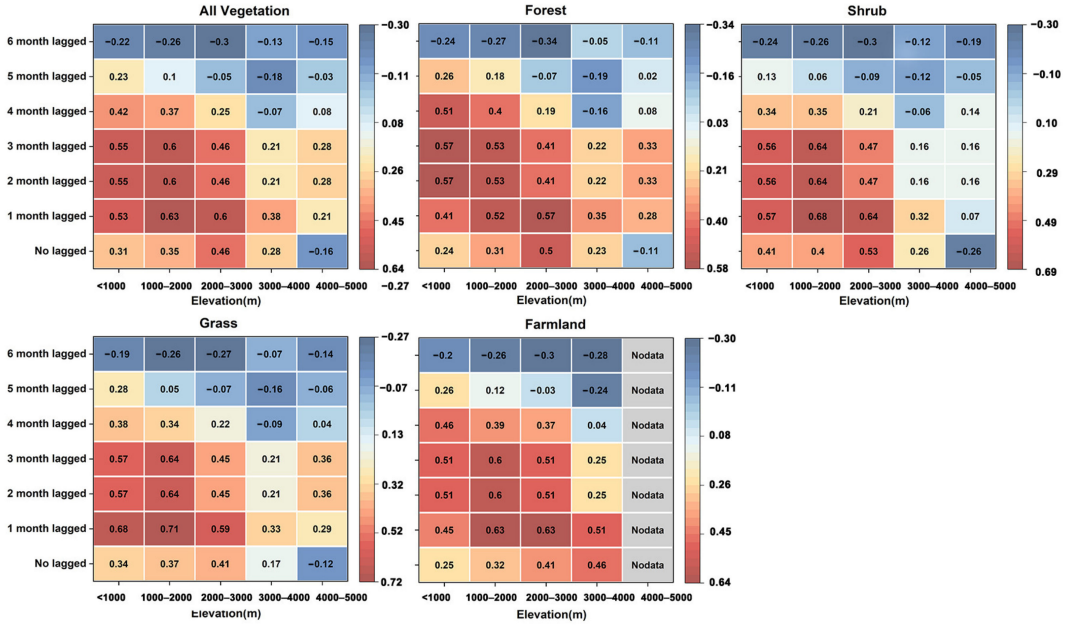

Figure 7. Correlation analysis of SPEI-3 and NPP for different vegetation types at different elevations.

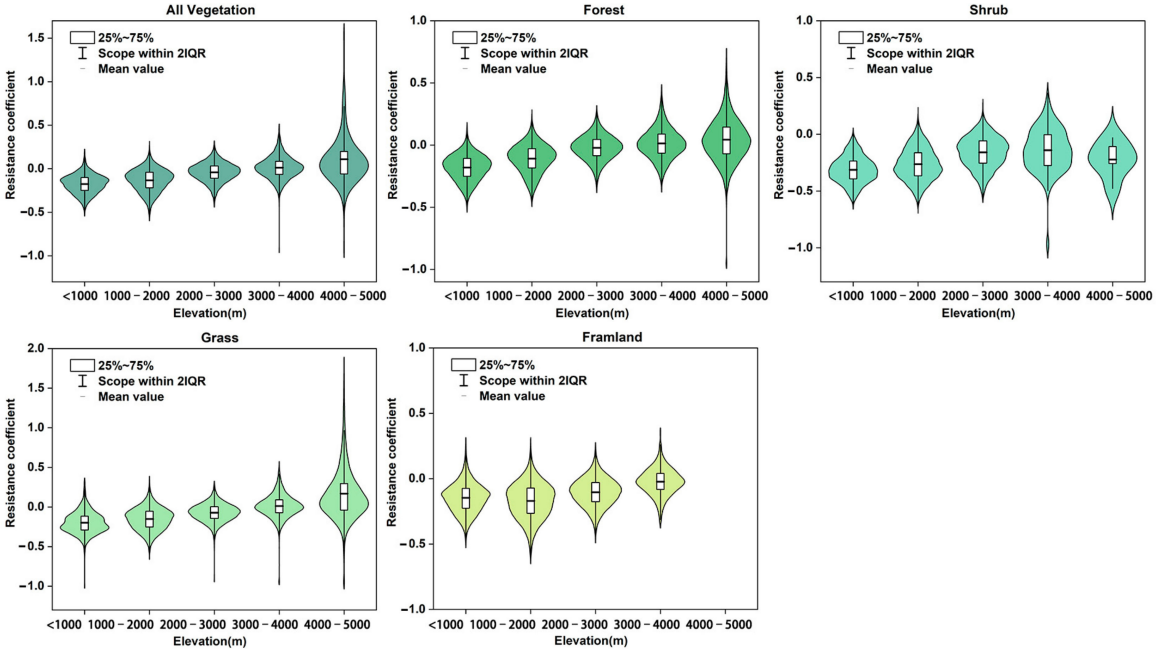

Figure 8. Resistance of different vegetation types to extreme drought at different elevations.

3.4. Vegetation's Recovery Ability from Extreme Drought

According to the research results from previous sections, there were no drought events in the Yunnan Plateau from 2007–2008 (Figure 3). To verify the reliability of the ARIMA model, we selected NPP inputs from 1982–2006 as the input data for the model to predict the NPP in 2007–2008 and compared it with the true NPP calculated by the CASA model. We selected R^2 and the root mean square error (RMSE) as indicators to evaluate the model accuracy, where a higher R^2 and a lower RMSE represent better model fitting. Figure 9 shows scatter plots of the NPP predicted by the ARIMA model and the NPP calculated by the CASA model for different vegetation types, as well as the changes in R^2 and RMSE for different monthly prediction lengths. The results show that the prediction accuracy of the ARIMA model, as measured by R^2, could reach above 0.8. When the prediction length

was more than five months, the R^2 and RMSE gradually stabilized, with R^2 maintained around 0.8. Except for shrubs, the RMSE of other vegetation types remained between 10–15, indicating that using the ARIMA model to predict the NPP during non-drought periods is feasible.

Figure 10 shows the recovery of vegetation for 1–24 months following extreme drought in the form of a waterfall chart. The vertical axis represents the corrected relative error (E_{Corr_error}), while the horizontal axis represents the months following the extreme drought. Through the vertical axis, we can clearly observe the changes in the growth and reduction in the corrected relative error. The first time E_{Corr_error} exceeds 0 (represented by the green bar in the histogram) signifies the time when vegetation productivity begins to recover. The results indicate that two years after the extreme drought, the recovery level ranks as follows: shrub > forest > grass > farmland. The residual effect of drought on all vegetation averages between 2–6 months. The residual effect of drought on forest vegetation occurs between 2–8 months, and low-elevation vegetation recovers more easily from extreme drought events. Recovery time for forest vegetation was two months at an elevation of 4000–5000 m, which may be due to the fact that high-elevation forest vegetation was less affected by this round of extreme drought and had a higher resistance. The residual effect of drought on shrub vegetation occurs between 2–8 months, and the recovery ability of medium–high elevation shrubs is better than that of low-elevation shrubs. Shrub vegetation above 3000 m can recover well from extreme drought events. The residual effect of drought on grassland vegetation occurs between 2–8 months, and the recovery of vegetation improves with increasing elevation. There is no significant difference between elevations for farmland vegetation, and its productivity begins to recover 8–14 months after extreme drought occurs.

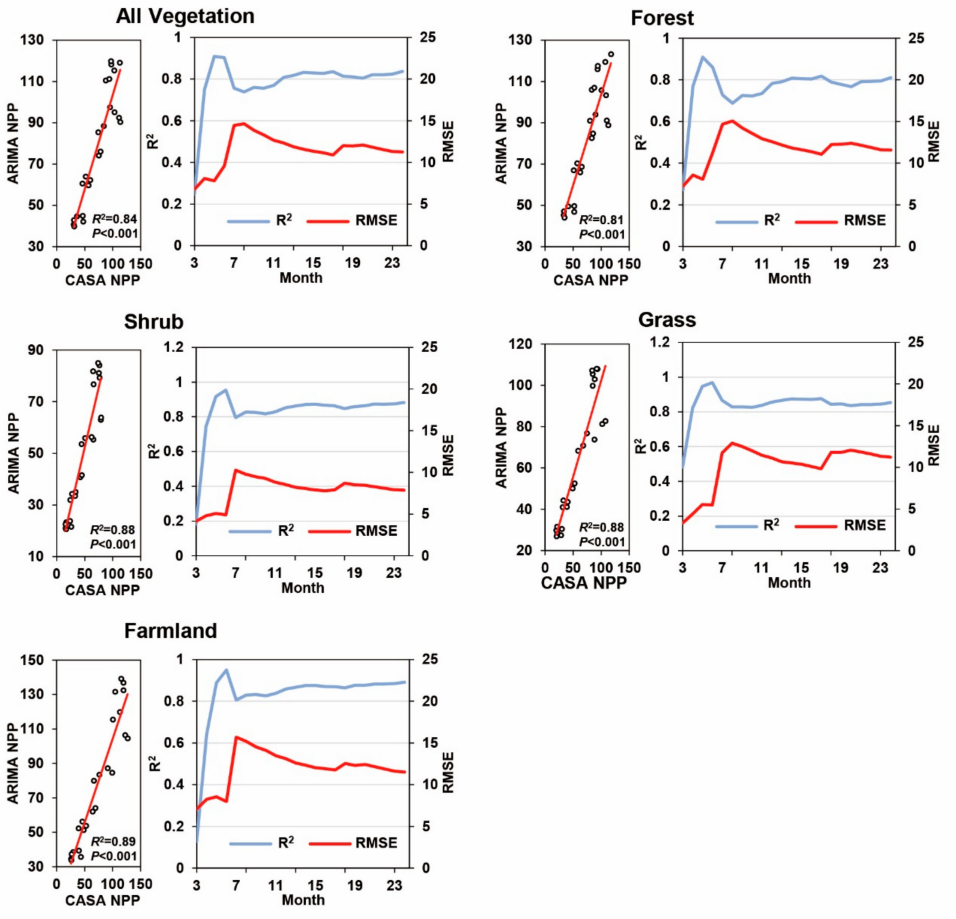

Figure 9. Reliability verification of ARIMA model.

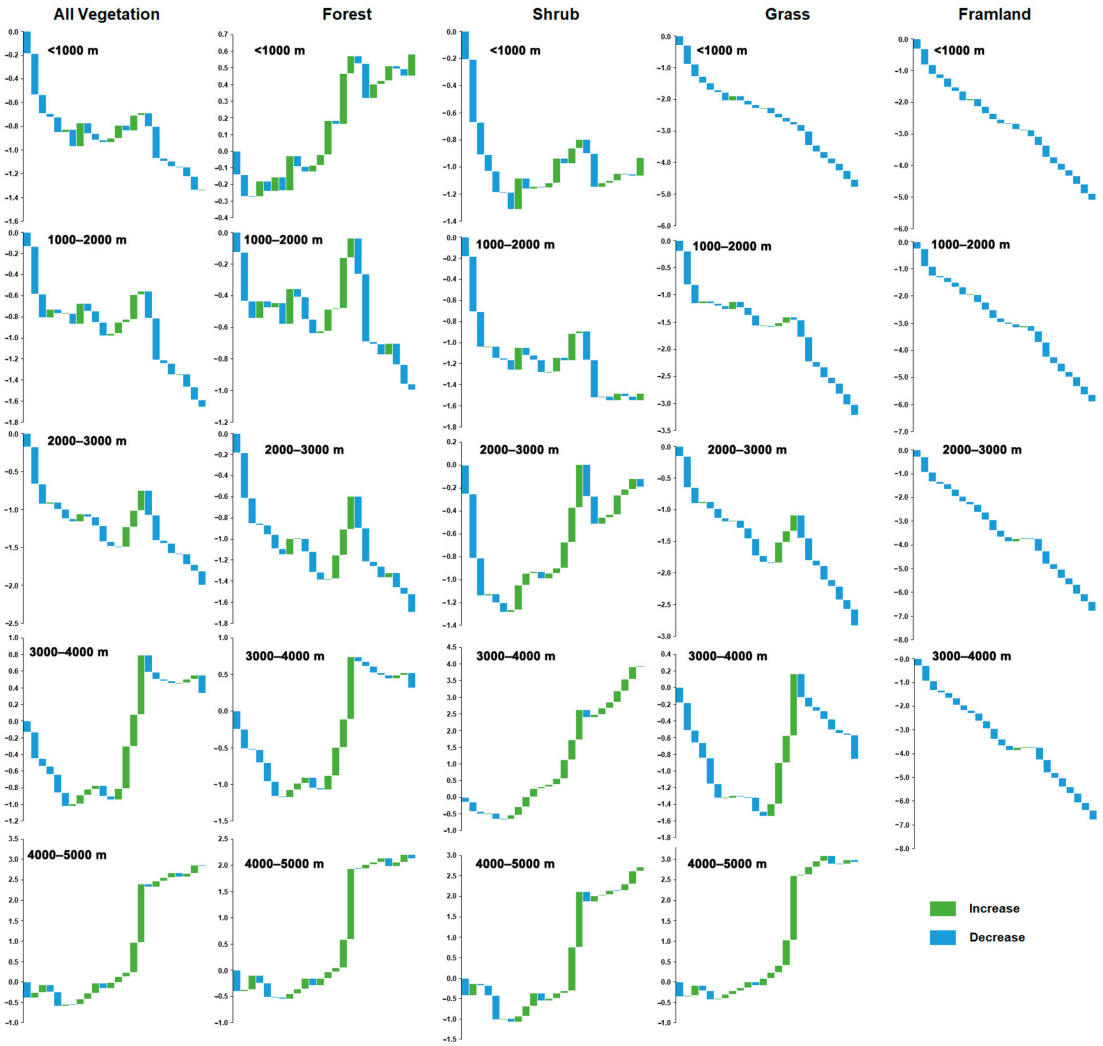

Figure 10. The resilience of vegetation to extreme drought.

4. Discussion

4.1. The Manifestations of Vegetation in Response to Extreme Drought

Yunnan is located in a low-latitude plateau region. Compared to other places at the same latitude, it has relatively less precipitation but higher evaporation, making it a relatively dry zone [44]. Anomalies in the circulation of the westerlies prevent the moisture from the Bay of Bengal from reaching the Yungui Plateau, resulting in less precipitation in Yunnan and causing an extreme drought event spanning autumn, winter, and spring [32,45]. During droughts, soil moisture decreases, which reduces the water available for plant photosynthesis. Additionally, plants close their stomata to reduce water loss, leading to a decrease in the intake of carbon dioxide by plant leaves, thereby reducing the rate of photosynthesis and ultimately resulting in a decline in the NPP of vegetation [46–48]. Simultaneously, the increased temperatures in winter and early spring cause an earlier onset of spring, leading to changes in vegetation structure and species composition. Therefore, extreme droughts cause a decline in NPP for that year, but the productivity can recover in a relatively short period of time [49].

Our research has found that different types of vegetation exhibit varying lag responses, resistance, and recovery abilities to extreme drought. Forest vegetation shows a slower response time to extreme drought compared to other types of vegetation but exhibits the highest resistance and relatively high recovery capabilities, second only to shrubs. This indicates that forests possess greater ecological stability in the face of extreme drought,

which is consistent with other research findings [26,50,51]. Current studies suggest that forests have deeper root systems, strong water retention capacities, and thicker leaves, reducing water evaporation. This allows them to regulate vegetation morphology and maintain photosynthetic efficiency during drought periods, giving them greater resistance and recovery abilities compared to other vegetation types [52,53]. Shrubs exhibit poorer resistance to extreme drought but have good recovery capabilities. This may be due to their relatively shallow and dispersed root systems, making it difficult for them to access deeper soil moisture sources. Additionally, their smaller leaf surface area cannot sustain water supply under drought conditions, leading to their lower resistance to extreme drought [54–56]. However, shrubs have shorter life cycles and good regenerative abilities in their roots and stems, allowing them to grow and reproduce quickly, thereby adapting to environmental changes and recovering faster from extreme drought events [57]. Grasslands exhibit good resistance to extreme drought, with a recovery period ranging from 2 to 8 months, which aligns with other research findings [58,59]. Farmland, being a human-controlled open system, has low biodiversity, a simple nutrient structure, and limited self-regulation abilities. As a result, it is highly vulnerable to damage during disturbances, leading to poor resistance and recovery capabilities to extreme drought [60,61].

4.2. The Impact of Elevation on Vegetation during Extreme Drought Events

Influenced by topographic patterns and monsoon systems, the Yunnan Plateau exhibits distinct climatic mountainous characteristics. Different altitudinal vegetation shows variations in response to extreme drought. This study found that for forest vegetation at elevations below 1000 m, the lag phase of response to extreme drought occurs around February to March. With increasing elevation, the lag phase advances, and the resistance increases. When the elevation exceeds 3000 m, the impact of extreme drought on vegetation weakens, and lower elevation vegetation demonstrates better recovery from extreme drought events compared to higher elevation vegetation. Shrub vegetation at elevations below 3000 m experiences a lag phase between 0 and 3 months, and resistance increases with elevation. Shrub vegetation at elevations between 3000 and 4000 m exhibits the highest resistance, and the recovery capability of shrubs at middle and high elevations is better than that of shrubs at lower elevation. Grassland vegetation at elevations below 3000 m is more susceptible to extreme drought, and resistance increases with elevation, along with better recovery. In general, vegetation in high-elevation regions is less susceptible to extreme drought, and resistance increases with elevation, which is consistent with other research findings [23,62]. Current studies indicate that NPP is influenced by temperature, precipitation, solar radiation, and the vegetation growth environment. Climate warming accelerates the thawing of permafrost in the northwestern part of Yunnan Plateau. The melting of snow at high elevation alleviates water loss and reduces the impact of drought on vegetation, leading to higher resistance to drought [63,64]. Precipitation and water use efficiency also affect plant recovery [22]. Low-elevation forests, mainly located in the southern part of the Yunnan Plateau, benefit from abundant rainfall, suitable temperatures, and higher water use efficiency, providing a favorable environment for forest growth [65]. As a result, the recovery capability of low-elevation forests exceeds that of high-elevation forests. The recovery level of agricultural vegetation is highly related to human cultivation and irrigation practices [59]. The provision of supplemental water through irrigation mitigates the impact of drought, resulting in no significant elevation differences in the recovery capability of agricultural vegetation.

4.3. Limitations and Prospects

The identification methods for extreme drought disasters are diverse, manifested in the diversity of drought indices and the uncertainty of drought thresholds. Common drought indices include precipitation, evaporation, SPI, and the SPEI used in this study. Drought is a complex phenomenon, and different drought indices identify and assess drought from different perspectives. A single index often cannot comprehensively evaluate

the impact of drought. Therefore, future research can employ a multi-index comprehensive approach to identify drought events, aiming to improve the accuracy and reliability of drought identification. At the same time, thresholds are critical in determining the severity of drought. However, drought thresholds are subjective and uncertain. In this study, we used the threshold of −1.5 as stipulated in the Chinese national standard. However, studies by other researchers have found that drought thresholds may vary in different regions. For example, Danandeh used a threshold of −1.83 for drought identification in Turkey [66]. Therefore, in future research, it is advisable to consider local climate, hydrological, and ecological characteristics for adjustment and optimization, as well as to conduct reasonable sensitivity analysis and validation of thresholds. Finally, this study did not consider other factors that may influence extreme drought events, such as soil properties, precipitation patterns, and human activities. In future research, these factors can be further taken into account to comprehensively evaluate the response of NPP to extreme drought.

5. Conclusions

Extreme drought periods resulted in a decrease in the NPP of Yunnan's vegetation. Vegetation exhibits a lag period of 1–3 months in response to extreme drought, with forests reacting slower than grasslands and shrubs, while also demonstrating higher resistance to extreme drought. Except for agricultural vegetation, other types of vegetation can start recovering their productivity within a year. Different altitudinal vegetation shows varied responses to extreme drought. Vegetation above 3000 m is less susceptible to the effects of extreme drought. As elevation increases, the lag period for forest vegetation in response to extreme drought advances, and resistance increases. Beyond 3000 m, the impact of extreme drought on vegetation weakens, and the residual effects on forest vegetation last between 2 and 8 months. Additionally, low-elevation vegetation is more capable of recovering from extreme drought events. For shrub vegetation below 3000 m, the lag period ranges from 0 to 3 months, and resistance increases with elevation, with the highest resistance occurring between 3000 and 4000 m. The residual effects of extreme drought on shrub vegetation persist between 2 and 8 months, with better recovery observed for mid–high elevation shrubs compared to low-elevation ones. Grassland vegetation below 3000 m exhibits a lag period of 1–3 months, while above 3000 m it shows a lower correlation with extreme drought. Vegetation resistance to drought increases with elevation, and the residual effects of extreme drought last between 2 and 8 months. As elevation increases, vegetation's recovery from extreme drought improves. For agricultural vegetation, the lag period ranges from 1 to 3 months, and mid–high elevation vegetation displays higher resistance. Recovery capacity does not show significant elevation differences, and the residual effects last between 8 and 14 months. Extreme drought events not only have a lag effect on the vegetation ecosystem, but also affect its stability and resilience to future drought events.

Author Contributions: Conceptualization, C.L. and Y.H.; methodology, C.L. and Y.H.; software, C.L.; validation, Z.W. and C.L.; formal analysis, Z.W.; writing—original draft preparation, C.L.; writing—review and editing, Y.H.; visualization, Z.W.; project administration, Y.H. All authors have read and agreed to the published version of the manuscript.

Funding: This research was supported by the National Natural Science Foundation of China (41961044), Yunnan University Postgraduate Scientific Research Innovation Project (KC-22221055).

Institutional Review Board Statement: Not applicable.

Informed Consent Statement: Not applicable.

Data Availability Statement: Not applicable.

Acknowledgments: The authors are grateful for the support of the National Natural Science Foundation of China (41961044).

Conflicts of Interest: The authors declare no conflict of interest.

References

1. Huang, J.; Ji, M.; Xie, Y.; Wang, H.; He, Y.; Ran, J. Global semi-arid climate change over last 60 years. *Clim. Dyn.* **2016**, *46*, 1131–1150. [CrossRef]
2. Ciais, P.; Reichstein, M.; Viovy, N.; Granier, A.; Ogée, J.; Allard, V.; Aubinet, M.; Buchmann, N.; Bernhofer, C.; Carrara, A.; et al. Europe-wide reduction in primary productivity caused by the heat and drought in 2003. *Nature* **2005**, *437*, 529–533. [CrossRef]
3. Craine, J.M.; Nippert, J.B.; Elmore, A.J.; Skibbe, A.M.; Hutchinson, S.L.; Brunsell, N.A. Timing of climate variability and grass-land productivity. *Proc. Natl. Acad. Sci. USA* **2012**, *109*, 3401–3405. [CrossRef]
4. Zhang, F.; Quan, Q.; Ma, F.; Tian, D.; Hoover, D.; Zhou, Q.; Niu, S. When does extreme drought elicit extreme ecological responses? *J. Ecol.* **2019**, *107*, 2553–2563. [CrossRef]
5. Schwalm, C.R.; Anderegg, W.R.L.; Michalak, A.M.; Fisher, J.B.; Biondi, F.; Koch, G.; Litvak, M.; Ogle, K.; Shaw, J.D.; Wolf, A.; et al. Global patterns of drought recovery. *Nature* **2017**, *548*, 202–205. [CrossRef]
6. Piao, S.; Zhang, X.; Chen, A.; Liu, Q.; Lian, X.; Wang, X.; Peng, S.; Wu, X. Effects of extreme climatic events on the carbon cycle of terrestrial ecosystems. *Sci. Sin. Terrae* **2019**, *49*, 1321–1334.
7. Field, C.B.; Behrenfeld, M.J.; Randerson, J.T.; Falkowski, P. Primary production of the biosphere: Integrating terrestrial and oceanic components. *Science* **1998**, *281*, 237–240. [CrossRef] [PubMed]
8. Halbac-Cotoara-Zamfir, R.; Smiraglia, D.; Quaranta, G.; Salvia, R.; Salvati, L.; Giménez-Morera, A. Land Degradation and Mitigation Policies in the Mediterranean Region: A Brief Commentary. *Sustainability* **2020**, *12*, 8313. [CrossRef]
9. Wang, X.; Wang, T.; Xu, J.; Shen, Z.; Yang, Y.; Chen, A.; Piao, S. Enhanced habitat loss of the Himalayan endemic flora driven by warming-forced upslope tree expansion. *Nat. Ecol. Evol.* **2022**, *6*, 890–899. [CrossRef]
10. Liu, X.; Guo, R.; Xu, X.; Shi, Q.; Li, X.; Yu, H.; Ren, Y.; Huang, J. Future increase in aridity drives abrupt biodiversity loss among terrestrial vertebrate species. *Earth's Future* **2023**, *11*, e2022EF003162. [CrossRef]
11. Li, J.; Wang, Z.; Wu, X.; Zscheischler, J.; Guo, S.; Chen, X. A standardized index for assessing sub-monthly compound dry and hot conditions with application in China. *Hydrol. Earth Syst. Sci.* **2021**, *25*, 1587–1601. [CrossRef]
12. Mohammed, S.; Alsafadi, K.; Enaruvbe, G.O.; Bashir, B.A.E.; Széles, A.; Alsalman, A.; Harsanyi, E. Assessing the impacts of agricultural drought (SPI/SPEI) on maize and wheat yields across Hungary. *Sci. Rep.* **2020**, *12*, 8838. [CrossRef]
13. Zhao, M.; Running, S.W. Drought-induced reduction in global terrestrial net primary production from 2000 through 2009. *Science* **2010**, *329*, 940–943. [CrossRef]
14. Mustafa Alee, M.; Danandeh Mehr, A.; Akdegirmen, O.; Nourani, V. Drought Assessment across Erbil Using Satellite Products. *Sustainability* **2023**, *15*, 6687. [CrossRef]
15. Fu, Y.H.; Zhao, H.; Piao, S.; Peaucelle, M.; Peng, S.; Zhou, G.; Ciais, P.; Huang, M.; Menzel, A.; Peñuelas, J.; et al. Declining global warming effects on the phenology of spring leaf unfolding. *Nature* **2015**, *526*, 104–107. [CrossRef]
16. Zhu, W.; Pan, Y.; Yang, X.; Song, G. Impact of climate change on net primary productivity of terrestrial vegetation in China. *Chin. Sci. Bull.* **2007**, *52*, 2535–2541. [CrossRef]
17. Quan, Q.; Tian, D.; Luo, Y.; Zhang, F.; Crowther, T.W.; Zhu, K.; Chen, H.; Zhou, Q.; Niu, S. Water scaling of ecosystem carbon cycle feedback to climate warming. *Sci. Adv.* **2019**, *5*, eaav1131. [CrossRef] [PubMed]
18. Green, J.K.; Berry, J.; Ciais, P.; Zhang, Y.; Gentine, P. Amazon rainforest photosynthesis increases in response to atmospheric dryness. *Sci. Adv.* **2020**, *6*, eabb7232. [CrossRef] [PubMed]
19. Saleska, S.R.; Didan, K.; Huete, A.R.; Da Rocha, H.R. Amazon forests green-up during 2005 drought. *Science* **2007**, *318*, 612. [CrossRef]
20. Nanzad, L.; Zhang, J.; Tuvdendorj, B.; Yang, S.; Rinzin, S.; Prodhan, F.A.; Sharma, T.P.P. Assessment of Drought Impact on Net Primary Productivity in the Terrestrial Ecosystems of Mongolia from 2003 to 2018. *Remote Sens.* **2021**, *13*, 2522. [CrossRef]
21. Cao, D.; Zhang, J.; Han, J.; Zhang, T.; Yang, S.; Wang, J.; Prodhan, F.A.; Yao, F. Projected increases in global terrestrial net primary productivity loss caused by drought under climate change. *Earth's Future* **2022**, *10*, e2022EF002681. [CrossRef]
22. Li, P.; Zhu, D.; Wang, Y.; Liu, D. Elevation dependence of drought legacy effects on vegetation greenness over the Tibetan Plateau. *Agric. For. Meteorol.* **2020**, *295*, 108190. [CrossRef]
23. Liu, L.; Wang, Y.; Wang, Z.; Li, D.; Zhang, Y.; Qin, D.; Li, S. Elevation-dependent decline in vegetation greening rate driven by increasing dryness based on three satellite NDVI datasets on the Tibetan Plateau. *Ecol. Indic.* **2019**, *107*, 105569. [CrossRef]
24. Knowles, J.F.; Scott, R.L.; Biederman, J.A.; Blanken, P.D.; Burns, S.P.; Dore, S.; Kolb, T.E.; Litvak, M.E.; Barron-Gafford, G.A. Montane forest productivity across a semiarid climatic gradient. *Glob. Chang. Biol.* **2020**, *26*, 6945–6958. [CrossRef]
25. Sun, H.; Wang, J.; Xiong, J.; Bian, J.; Jin, H.; Cheng, W.; Li, A. Vegetation Change and Its Response to Climate Change in Yunnan Province, China. *Adv. Meteorol.* **2021**, *2021*, 8857589. [CrossRef]
26. Shao, H.; Zhang, Y.; Yu, Z.; Gu, F.; Peng, Z. The Resilience of Vegetation to the 2009/2010 Extreme Drought in Southwest China. *Forests* **2022**, *13*, 851. [CrossRef]
27. Wang, W.; Wang, W.J.; Li, J.S.; Wu, H.; Xu, C.; Liu, X.F.; Liu, T. Remote Sensing Analysis of lmpacts of Extreme Drought Weather on Ecosystems in Southwest Region of China Based on Normalized DifferenceVegetation Index. *Res. Environ. Sci.* **2010**, *23*, 1447–1455.
28. Zhao, Z.P.; Wu, X.P.; Li, G.; Li, J.S. Drought in southwestern China and its impact on the net primary productivity of vegetation from 2009–2011. *Acta Ecol. Sin.* **2015**, *35*, 350–360.

29. Yan, W.B.; He, Y.L.; Yu, L.; Qu, X.X. Effect of drought on net primary productivity of vegetation in Yunnan Province. *J. Yunnan Univ. Nat. Sci. Ed.* **2021**, *43*, 736–745.
30. Han, L.; Zhang, Q.; Yao, Y.; Li, Y.; Jia, J.; Wang, J. Characteristics and origins of drought disasters in Southwest China in nearly 60 years. *Acta Geogr. Sin.* **2014**, *69*, 632–639.
31. Yin, H.; Li, Y. Summary of Advance on Drought Study in Southwest China. *J. Arid Meteorol.* **2013**, *31*, 182–193.
32. Huang, R.; Liu, Y.; Wang, L.; Wang, L. Analyses of the Causes of Severe Drought Occurring in Southwest China from the Fall of 2009 to the Spring of 2010. Chin. *J. Atmos. Sci.* **2012**, *36*, 443–457. [CrossRef]
33. Liu, J.; Yan, H.; Li, Y. Analysis of the circulation influencing factors of the abnormal high temperature and drought in Yunnan in the early summer of 2019. *Yunnan Geogr. Environ. Res.* **2020**, *32*, 42–48. [CrossRef]
34. Tong, C.; Zhang, W.; Tang, Y.; Wang, H. Estimation of Daily Solar Radiation in China. *Chin. J. Agrometeorol.* **2005**, *26*, 165–169. [CrossRef]
35. Hutchinson, M.F. *ANUSPLIN Version 4.3 User Guide*; The Australia National University, Center for Resource and Environment Studies: Canberra, Australia, 2004; Available online: https://fennerschool.anu.edu.au/research/products/anusplin (accessed on 1 January 2023).
36. Liu, Z.H.; Tim, R.; Van, N.; Yang, Q.K.; Li, R. Introduction of the Professional Interpolation Software for Meteorology Data: ANUSPLINN. *Meteorol. Mon.* **2008**, *398*, 92–100.
37. Parra, J.L.; Monahan, W.B. Variability in 20th century climate change reconstructions and its consequences for predicting geographic responses of California mammals. *Glob. Chang. Biol.* **2008**, *14*, 2215–2231. [CrossRef]
38. Feng, L.; Liu, Y.X.; Feng, Z.Z.; Yang, S.Q. Analysing the spatiotemporal characteristics of climate comfort in China based on 2005–2018 MODIS data. *Theor. Appl. Climatol.* **2021**, *143*, 1235–1249. [CrossRef]
39. Wu, W.; Liu, Q.; Li, H.; Huang, C. Spatiotemporal Distribution of Heatwave Hazards in the Chinese Mainland for the Period 1990–2019. *Int. J. Environ. Res. Public Health* **2023**, *20*, 1532. [CrossRef]
40. Ma, Z.; Dong, C.; Lin, K.; Yan, Y.; Luo, J.; Jiang, D.; Chen, X. A Global 250-m Downscaled NDVI Product from 1982 to 2018. *Remote Sens.* **2022**, *14*, 3639. [CrossRef]
41. Yang, J.; Huang, X. The 30 m annual land cover dataset and its dynamics in China from 1990 to 2019. Earth Syst. *Sci. Data* **2021**, *13*, 3907–3925. [CrossRef]
42. Vicente-Serrano, S.M.; Beguería, S.; López-Moreno, J.I. A multiscalar drought index sensitive to global warming: The standardized precipitation evapotranspiration index. *J. Clim.* **2010**, *23*, 1696–1718. [CrossRef]
43. Box, G. *Time Series Analysis, Forecasting and Control*; Holden-Day: San Francisco, CA, USA, 1976.
44. Wang, J.; Sun, H.; Xu, W.; Zhou, J. Spatio-temporal change of drought disaster in China in recent fifty years. *J. Nat. Disasters* **2002**, *11*, 1–6. [CrossRef]
45. Yang, H.; Song, J.; Yan, H.; Yin, L. Cause of the severe drought in Yunnan Province during winter of 2009 to 2010. *Clim. Environ. Res.* **2012**, *17*, 315–326. (In Chinese) [CrossRef]
46. Passioura, J.B. The yield of crops in relation to drought. In *Physiology and Determination of Crop Yield*; American Society of Agronomy: Maddison, WI, USA, 1994; pp. 343–359. [CrossRef]
47. Cramer, M.D.; Hawkins, H.J.; Verboom, G.A. The importance of nutritional regulation of plant water flux. *Oecologia* **2009**, *161*, 15–24. [CrossRef] [PubMed]
48. Stocker, B.D.; Zscheischler, J.; Keenan, T.F.; Prentice, I.C.; Seneviratne, S.I.; Peñuelas, J. Drought impacts on terrestrial primary production underestimated by satellite monitoring. *Nat. Geosci.* **2019**, *12*, 264–270. [CrossRef]
49. Chen, Y.; Feng, X.; Tian, H.; Wu, X.; Gao, Z.; Feng, Y.; Piao, S.; Lv, N.; Pan, N.; Fu, B. Accelerated increase in vegetation carbon sequestration in China after 2010: A turning point resulting from climate and human interaction. *Glob. Chang. Biol.* **2021**, *27*, 5848–5864. [CrossRef]
50. Abbas, S.; Nichol, J.E.; Qamer, F.M.; Xu, J. Characterization of Drought Development through Remote Sensing: A Case Study in Central Yunnan, China. *Remote Sens.* **2014**, *6*, 4998–5018. [CrossRef]
51. Huang, K.; Xia, J. High ecosystem stability of evergreen broadleaf forests under severe droughts. *Glob. Chang. Biol.* **2019**, *25*, 3494–3503. [CrossRef] [PubMed]
52. Wu, J.; Albert, L.P.; Lopes, A.P.; Restrepo-Coupe, N.; Hayek, M.; Wiedemann, K.T.; Guan, K.; Stark, S.C.; Christoffersen, B.; Prohaska, N.; et al. Leaf development and demography explain photosynthetic seasonality in Amazon evergreen forests. *Science* **2016**, *351*, 972–976. [CrossRef] [PubMed]
53. Muñoz, R.; Bongers, F.; Rozendaal, D.M.A.; González, E.J.; Dupuy, J.M.; Meave, J.A. Autogenic regulation and resilience in tropical dry forest. *J. Ecol.* **2021**, *109*, 3295–3307. [CrossRef]
54. Schenk, H.J.; Jackson, R.B. Rooting depths, lateral root spreads and below-ground/above-ground allometries of plants in water-limited ecosystems. *J. Ecol.* **2002**, *90*, 480–494. [CrossRef]
55. Kulmatiski, A.; Adler, P.; Foley, M. Hydrologic niches explain species coexistence and abundance in a shrub–steppe system. *J. Ecol.* **2019**, *108*, 998–1008. [CrossRef]
56. Barbeta, A.; Mejía-Chang, M.; Ogaya, R.; Voltas, J.; Dawson, T.E.; Peñuelas, J. The combined effects of a long-term experimental drought and an extreme drought on the use of plant-water sources in a Mediterranean forest. *Glob. Chang. Biol.* **2015**, *21*, 1213–1225. [CrossRef] [PubMed]

57. Lortie, C.J.; Gruber, E.; Filazzola, A.; Noble, T.; Westphal, M. The Groot Effect: Plant facilitation and desert shrub regrowth following extensive damage. *Ecol. Evol.* **2018**, *8*, 706–715. [CrossRef] [PubMed]
58. Shinoda, M.; Nachinshonhor, G.U.; Nemoto, M. Impact of drought on vegetation dynamics of the Mongolian steppe: A field experiment. *J. Arid. Environ.* **2010**, *74*, 63–69. [CrossRef]
59. Li, X.; Li, Y.; Chen, A.; Gao, M.; Slette, I.J.; Piao, S. The impact of the 2009/2010 drought on vegetation growth and terrestrial carbon balance in southwest china. *Agric. For. Meteorol.* **2019**, *269–270*, 239–248. [CrossRef]
60. Yin, F.; Mao, R.Z.; Fu, B.J.; Liu, G.H. Farmland ecosystem service and its formation mechanism. *Chin. J. Appl. Ecol.* **2006**, *5*, 929–934.
61. Lesk, C.; Rowhani, P.; Ramankutty, N. Influence of extreme weather disasters on global crop production. *Nature* **2016**, *529*, 84–87. [CrossRef]
62. Rita, A.; Camarero, J.J.; Nolè, A.; Borghetti, M.; Brunetti, M.; Pergola, N.; Serio, C.; Vicente-Serrano, S.M.; Tramutoli, V.; Ripullone, F. The impact of drought spells on forests depends on site conditions: The case of 2017 summer heat wave in southern Europe. *Glob. Chang. Biol.* **2020**, *26*, 851–863. [CrossRef]
63. Wu, X.; Li, X.; Liu, H.; Ciais, P.; Li, Y.; Xu, C.; Babst, F.; Guo, W.; Hao, B.; Wang, P.; et al. Uneven winter snow influence on tree growth across temperate China. *Glob. Chang. Biol.* **2019**, *25*, 144–154. [CrossRef]
64. Wang, Y.; Fu, B.; Liu, Y.; Li, Y.; Feng, X.; Wang, S. Response of vegetation to drought in the Tibetan Plateau: Elevation differentiation and the dominant factors. *Agric. For. Meteorol.* **2021**, *306*, 108468. [CrossRef]
65. Zhang, Y.; Shui, W.; Sun, X.; Sun, X. Spatiotemporal variation and influencing factors of vegetation water use efficiency in Yunnan Province. *Acta Ecol. Sin.* **2022**, *42*, 2405–2417. [CrossRef]
66. Danandeh Mehr, A.; Vaheddoost, B. Identification of the trends associated with the SPI and SPEI indices across Ankara, Turkey. *Theor. Appl. Climatol.* **2020**, *139*, 1531–1542. [CrossRef]